JOURNAL OF MATERIALS SCIENCE 28 (1993) 6127–6135

Al_2O_3-and ZrO_2-modified dental glass ceramics

J. M. TZENG, J. G. DUH
Department of Materials Science and Engineering, National Tsing Hua University, Hsinchu, Taiwan

K. H. CHUNG AND C. C. CHAN
Dental Department, Veterans General Hospital, Taipei, Taiwan

Castable machinable glass-ceramics have been widely considered as aesthetic materials for dental restoration. In order to extend their applications to bridge-work fabrication, it is necessary to increase their fracture strength and fracture toughness. The effects of ziconia and alumina additions on the properties of glass-ceramics, especially on the mechanical properties were studied. It was found that appropriate addition of alumina increases the bending strength due to aluminium strengthening the glass-ceramic by means of incorporation into the glass network. However, additions of ziconia fail to show promising results on the mechanical property. The evolution of recrystallization and the associated microstructure were also studied and are discussed.

1. Introduction

Glass-ceramics are polycrystalline solids that are produced by controlled crystallization of glass. Owing to their chemical inertness combined with high mechanical strength, appropriate thermal and physical properties [1, 2], glass-ceramics have generated interest in applications in the biomedical field, especially in the replacement of natural bone and dental restoration [3]. The potential of using glass-ceramics for dental applications was first introduced by MacCulloch [4] in 1968. The first demonstrated use of a castable glass-ceramic system for the fabrication of restorations was reported by Hench *et al.* in 1971 [5]. The use of a machinable glass-ceramic that can be melted and cast into the form of dental inlays, onlays and crowns was introduced by Adair [6] and Grossman [7]. This product, which is marketed under the commercial name DICOR, is developed by Dentsply International in conjunction with Corning Glass Works.

DICOR with compositions enriched in K_2O and SiO_2 can be melted from 1350–1400 °C and subsequently be cerammed to yield a tetrasilicic fluorine mica ($KMg_{2.5}Si_4O_{10}F_2$) glass-ceramic [8]. The mica crystals grow by a dissolution and reprecipitation mechanism at 1075 °C. A holding time of 6 h is considered optimum for strength and other desirable properties. The machinability of DICOR glass-ceramic results from microstructures consisting of easily cleavable mica flakes uniformly dispersed in a glass matrix and a weak interface between crystalline and glass phase. In addition to machinability, DICOR glass-ceramic can retain a high degree of translucency even if a ceramming process is carried out. The reason may be due to the fineness of crystals formed and the fact that the refractive index of the glass is close to that of precipitated crystals.

DICOR glass-ceramic possesses better mechanical properties over other glass-ceramics already used in dental restoration [9]. However, because of its limitation in strength and fracture toughness, no bridge-work fabrication is yet recommended. In recent years, the intensive studies of ziconia and alumina have developed them into versatile materials. Ziconia and alumina have high strength, high fracture toughness, and high modulus of elasticity, which are advantageous for reinforcing the glass-ceramic materials. It is thought that glass-ceramic materials may be strengthened or toughened by means of the so-called transformation toughening through the phase transformation of ZrO_2 or ZrO_2–Al_2O_3 composite [10, 11].

The purpose of this study was to investigate the effects of ZrO_2 and Al_2O_3 additions on the mechanical properties of DICOR modified system. Simulated formulations were fabricated and their properties were evaluated. X-ray diffraction, SEM, EPMA, NMR, and indentation hardness tests were employed to investigate the physical and mechanical properties of the as-derived modified DICOR system.

2. Experimental procedure

In addition to commercialized DICOR glass (Dentsply International and Corning Glass Works), there were three types of glass employed in this study. A simulated composition to DICOR was the first one used and called SDICOR. The second type, SDZR05, SDZR10 and SDZR20, contained 5%, 10%, and 20% extra ZrO_2, respectively, compared to the simulated composition. In the third type of glass, Al_2O_3 was applied as the extra dopant in SDAL100, SDAL200 and SDAL300, in which 100%, 200%, and 300% more Al_2O_3, respectively, was added than that in the simulated SDICOR composition. Table I summarizes the nominal compositions of the glass employed in this experiment.

0022–2461

TABLE I Nominal composition of DICOR related glass-ceramics (wt %)

Sample	SiO_2	K_2CO_3	MgO	MgF_2	ZrO_2	Al_2O_3
SDICOR	55.92	19.12	8.76	10.95	4.76	0.49
SDZR05	55.92	19.12	8.76	10.95	5.00	0.49
SDZR10	55.92	19.12	8.76	10.95	5.24	0.49
SDZR20	55.92	19.12	8.76	10.95	5.71	0.49
SDAL100	55.92	19.12	8.76	10.95	4.76	0.98
SDAL200	55.92	19.12	8.76	10.95	4.76	1.47
SDAL300	55.92	19.12	8.76	10.95	4.76	1.96

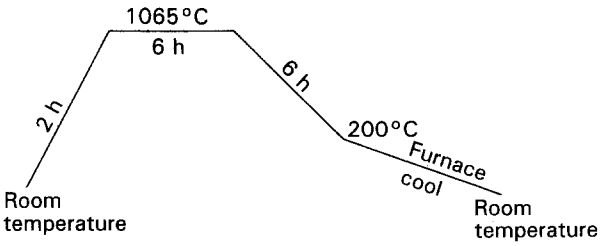

Figure 1 Heat-treatment process of the ceramming procedure.

A batch of powders was prepared by mixing SiO_2, K_2CO_3, MgO, MgF_2, ZrO_2, and Al_2O_3 in ethyl alcohol with ZrO_2 balls in a PE jar. After 4 h mixing, the batch was dried under an infrared lamp on a magnetic-stirring hot plate. After drying, the powder was melted at 1470–1500 °C for 2 h in a platinum crucible, then the molten liquid was quenched on to a copper plate. The as-fabricated bulk glass was annealed at 550–650 °C for 1 h in order to relieve thermal stress induced by the quenching process.

The casting process was performed by first heating, melting, and then centrifugal casting in DICOR casting machine. The casting temperature was 1365 °C. The as-cast samples were 20 mm × 15 mm × 4 mm in size. After cleaning the investment material, the ingot was sandblasted with 1 μm Al_2O_3 and followed by ultrasonically cleaning for 10 min in the distilled water. Sandblasting is necessary to minimize any possible line of cleavage and residual cracks that have been created during previous treatment.

The cast ingot of glass should be heat treated, i.e. cerammed, to develop optimum physical and mechanical properties. The ingot was embedded in a DICOR castable ceramming investment during the ceramming process to ensure dimensional accuracy as well as to maintain uniform temperature distribution around the ingot. The ceramming profile is indicated in Fig. 1.

X-ray phase analysis was performed with a X-ray diffractometer (D/MAX-B, Rigaku, Japan) equipped with CuK_α radiation and a nickel filter. A scan speed of 2° min^{-1} was used.

Thermal analysis included differential thermogravimetry (DTG), differential thermal analysis (DTA), and dilatometer test (DL) in a thermal analyser (ULVAC TGD-7000 and DL-7000). DTG and DTA were carried out to 1100 °C with a heating rate of 10 °C min^{-1}. DL was performed to 800 °C for glass and to 400 °C for as-cerammed specimens, respectively, with the same heating rate as DTA.

The strength of the as-cerammed sample was evaluated by three-point bending tests in a MTS tensile machine (MTS 810 Material Test System, MN, USA). The crosshead speed was 3 mm/min^{-1}. The sample size for the bending test is 15 mm × 4 mm × 3 mm, with the upper surface ground to 1200 SiC paper, and the lower surface polished to 1 μm diamond paste. The bending strength is estimated according to

$$\sigma_{3p} = \frac{3PL}{2wt^2} \quad (1)$$

where σ_{3p} is the strength (MPa), P the fracture load (N), L the span length (mm), t the specimen thickness (mm), and w the specimen width (mm).

The microstructures of the as-cast and cerammed specimens were examined with a scanning electron microscope (250 MK3, Cambridge, UK). Further investigations of elemental distribution were performed with an electron probe microanalyzer (EPMA 733, Jeol, Japan). Before SEM and EPMA examination, samples were ground by SiC papers of 1200 grade, followed by polishing with 6 and 1 μm diamond pastes to produce a optically-refractive surface. 1.5 wt% HF (1.5 HF + 98.5 deionized water by weight) was chosen as the etching solution. Etching was carried out at room temperature for 10–15 s to obtain a visible microstructure. A thin layer of gold was coated on the polished surface for SEM examination while a thin layer of carbon film was applied for EPMA analysis.

3. Results and discussion

3.1. Density and phases

Density is calculated by Archimedes method with deionized water as the medium. The densities of glass and as-cerammed samples are listed in Table II. The density of as-cerammed DICOR is 2.69 g/cm^{-3}, which is close to the value (2.7 g/cm^{-3}) reported by Dentsply International and Corning Glass Works [12]. Densities of as-cerammed samples listed in Table II are nearly the same. However, there exists a slight difference among glass samples. The difference may primarily arise from the cooling and the annealing process. Take SDZR20 as an example. A higher glass density is mainly due to the effect of the over-annealing process in which fine mica crystals have formed. The over-annealing process corresponds to a lower cooling rate when the glass is quenched, and thus a higher glass density is attained. In addition, the higher density may be attributed to the presence of the precipitated mica phase.

The X-ray pattern was obtained in a diffractometer with a copper target, in which the scan speed was set at 2° min^{-1} to minimize the background and noise interruption. Bulk samples were originally used as tested specimens, but severe angle shifting was induced because of the unflat surface. More accurate results could be derived by the employment of powder samples. Fig. 2a shows the X-ray diffraction pattern of commercialized DICOR after ceramming. By comparison with JCPDS (Joint Committee on Powder Diffraction Standards) cards, the diffraction angles are close to the tetrasilicic hydroxyl mica ($KMg_{2.5}Si_4O_{10}$

TABLE II Densities of glass and as-cerammed DICOR-related systems

	Density (g cm^{-3})	
	Glass	As-cerammed
DICOR	2.52	2.69
SDICOR	2.54	2.69
SDZR05	2.58	2.67
SDZR10	2.47	2.68
SDZR20	2.64	2.70
SDAL100	2.55	2.67
SDAL200	2.57	2.66
SDAL300	2.57	2.69

$(OH)_2$). The name "tetrasilicic" is derived from the crystal chemistry of the precipitated mica crystals [8]. The silicate sheets of the structure are formed entirely from SiO_4 tetrahedra, because no trivalent cations such as B^{3+} and Al^{3+} are present to substitute for silicon. Thus, the fluorine mica crystals that own the postulated formula $KMg_{2.5}Si_4O_{10}F_2$ are synthetic mica crystals with a structure similar to fluorophlogpite ($KMg_3\ AlSi_3\ O_{10}\ F_2$) and boron fluorophlogpite ($KMg_3\ BSi_3O_{10}F_2$). The diffraction pattern of $KMg_{2.5}Si_4O_{10}F_2$ is also close to the pattern described by Seifert and Schreyer [13]. In Grossman's argument [8], fluorine mica is the product that F substitutes hydroxyl mica to form $KMg_{2.5}Si_4O_{10}F_2$ fluorine mica. Because these mica crystals possess similar X-ray diffraction patterns, the indexes of fluorine mica crystalline planes match those of hydroxyl mica phase.

The X-ray diffraction patterns of SDICOR, SDZR20, and SDAL200 are illustrated in Fig. 2 b–d, respectively. After peak identification, it appears that mica crystals form in those four systems. However, the simulated systems contain an unidentified peak around 28.2° (2θ), which may represent either ZrO_2 or $MgSiO_3$. According to Grossman, enstatite ($MgSiO_3$) would form for the low K_2O–high MgO system at $\approx 980\,^\circ C$ in addition to tetrasilicic fluorine mica. The enstatite does not interfere with the glass machinability but has the added benefit of increasing the refractories of the material [8]. In comparing with JCPDS cards, (420) and (610) peaks of $MgSiO_3$ match the unidentified peak in the X-ray pattern of simulated systems, although there is small peak shift around 0.1–0.3 in 2θ. Nevertheless, Grossman reported that $MgSiO_3$ formed at $\approx 980\,^\circ C$, but in this study the observed peak at $2\theta = 28.2^\circ$ occurred at $800\,^\circ C$, heat treatment for 2 h. Thus, it is difficult to conclude the presence of $MgSiO_3$. There is another possibility for the unknown peak to be monoclinic ZrO_2 (m-ZrO_2), instead of $MgSiO_3$. It is observed that the larger the ZrO_2 dopants, the higher is the ratio of peak intensity for the unknown to (003) $KMg_{2.5}Si_4O_{10}F_2$ [14]. For the present time, the phase at $2\theta = 28.2^\circ$ still remains unresolved.

3.2. Evaluation of thermal properties

3.2.1. Glass Transition temperature, (T_g)

The glass transition temperatures were evaluated by thermal expansion measurement. The results are given

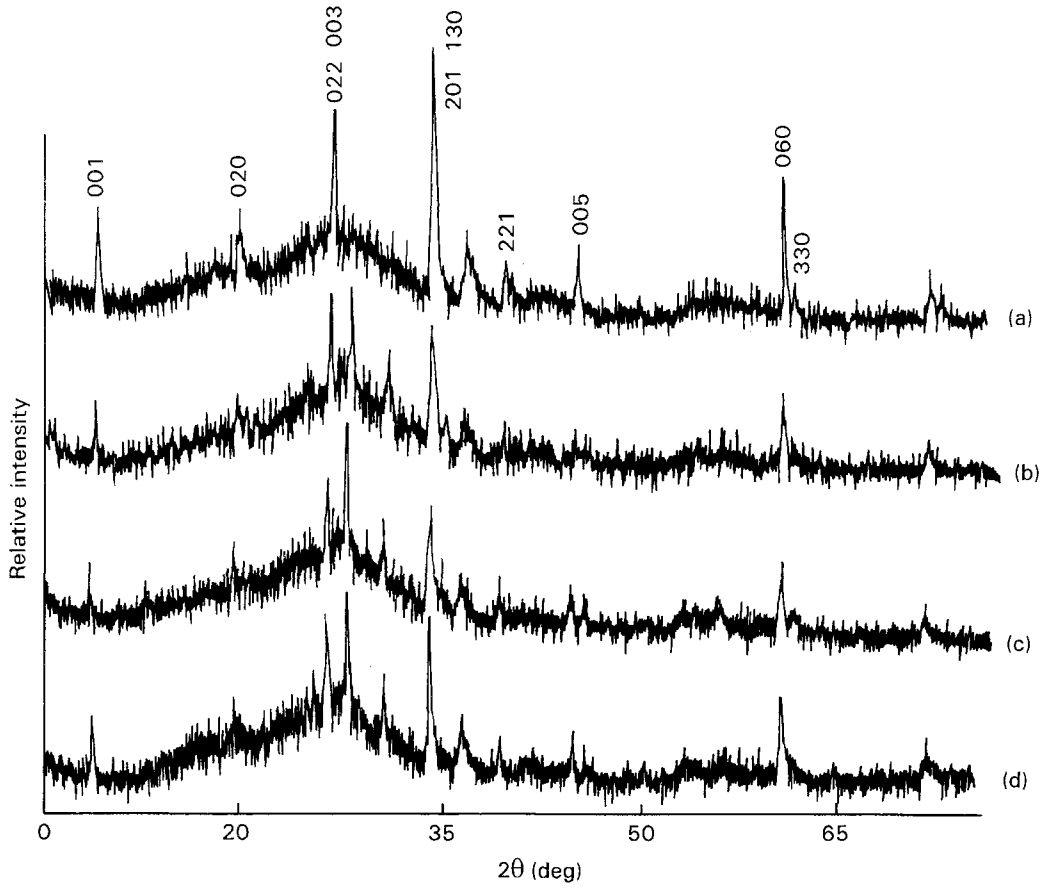

Figure 2 X-ray diffraction patterns of DICOR-related glass.

in Table III. The glass transition temperature, T_g, is the temperature at which atomic motions become sufficient to allow stress relaxation. From Table III, it is apparent that extra additions of ZrO_2 and Al_2O_3 do not change T_g significantly. This implies that the structure and bonding of the raw glass are not altered by these additives and neither are the thermal properties and viscosity of the glass.

3.2.2. Crystallization peak temperature, T_c

Crystallization temperature was determined from the DTA curve, and the T_c is defined as the point of maximum crystallization rate, as shown in Fig. 3. The results are listed in Table IV. It should be pointed out that extra additions of Al_2O_3 and ZrO_2 are considered to be the intermediate glass formers. They are incorporated into the glass network and tend to increase the stability of the glass [15]. Thus T_c is enhanced as indicated in Table IV.

3.3. Microstructure analysis

Microstructure observation was carried out in a scanning electron microscope (SEM) and electron probe microanalyser (EPMA). Pre-treatments of samples included grinding, polishing, and etching. A better morphology contrast can be achieved with a solution containing 1.5 wt% HF, and the etching time was 15 s. The purpose of etching is to develop a visible image contrast by means of difference in corrosion resistance of different phases to the etching solution. Glass-ceramics in which a crystalline phase is precipitated from a glass phase, contain crystalline and residual glass phase. Owing to the difference in corrosion resistance to the etching solution, either the glass phase or the crystalline phase will be etched by the etching solution, and then a visible image contrast between glass phase and crystalline phase is produced. In this study, the glass phase is less corrosive-resistant than the crystalline phase if HF is used as an etching solution. Fig. 4 represents the typical microstructure of as-cerammed DICOR-related glass. In general, the mica grain grows by the dissolution and precipitation mechanism. According to Grossman [8], the mica phase crystallizes as small spherical grains ($\sim$ 40 nm) at 625 °C and crystallizes into a larger booklet at 940 °C. The book-like morphology is produced by reducing the thermal stress induced from strong anisotropy in thermal expansion. Fine grains with low aspect ratio (aspect ratio = diameter/thickness) will effectively minimize the thermal mismatch.

In addition to fine grains, there exist large-size and higher aspect grains among the DICOR and other simulated systems, especially for SDZR20. The morphology of these abnormal grains is highlighted in Fig. 4c. Apparent differences between fine grains and abnormal grains are the grain size and aspect ratio. For fine grains, the grain size is smaller than 2 μm, and the aspect ratio is near 1. For abnormal grain, however, the grain size is larger than 5 μm and the aspect ratio is greater than 5. On some occasions, a grain size larger than 10 μm can be found.

At lower magnification in SEM observation, both fine grains and abnormal grains are visible, as illustrated in Fig. 5. Two distinct regions exist in Fig. 5a. The darker region represents the accumulation of large-size grains, in which grains agglomerate together. Fig. 5b and c show the area at higher magnification. The lighter region in Fig. 5a is the area associated with fine grains. Distinction in refractive index between glass phase and crystalline phase is responsible for the image difference in Fig. 5a. A glass-ceramic will lose its transparency when the ceramming process is carried out because of the difference in the refractive index between raw glass and precipitated crystals. The glass-ceramic can remain translucent if fine grains are precipitated, but will turn opaque when large grains appear [16]. Because it turns opaque due to the large grain-size effect, the darker area corresponds to the region of abnormal grain assembly.

According to Fig. 5c more glass phase but fewer fine grains exist in the neighborhood of the abnormal grain region than in the fine grain region. The reason may be discussed as follows. In general, the abnormal grains grow from pre-formed nuclei or grains after casting. As the ceramming process proceeds these pre-formed nuclei and grains will grow at a higher rate

TABLE III Transition temperature of DICOR-related glass

Sample	T_g (°C)
DICOR	608
SDICOR	660
SDZR05	655
SDZR10	655
SDAL100	655
SDAL200	650

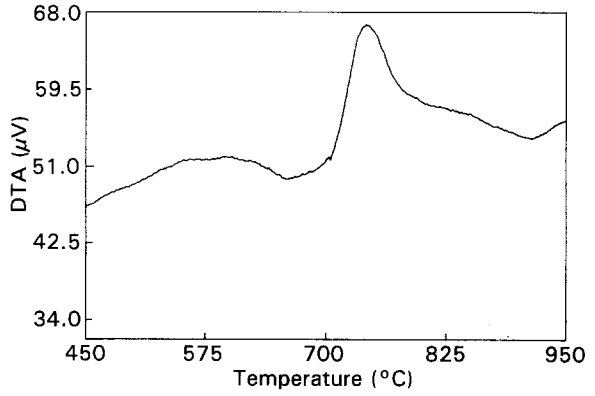

Figure 3 DTA curve of SDICOR glass.

TABLE IV Crystalilization temperature of DICOR-related glass

Sample	T_g (°C)
DICOR	694
SDICOR	743
SDZR05	796
SDZR10	796
SDAL100	813
SDAL200	818
SDAL300	834

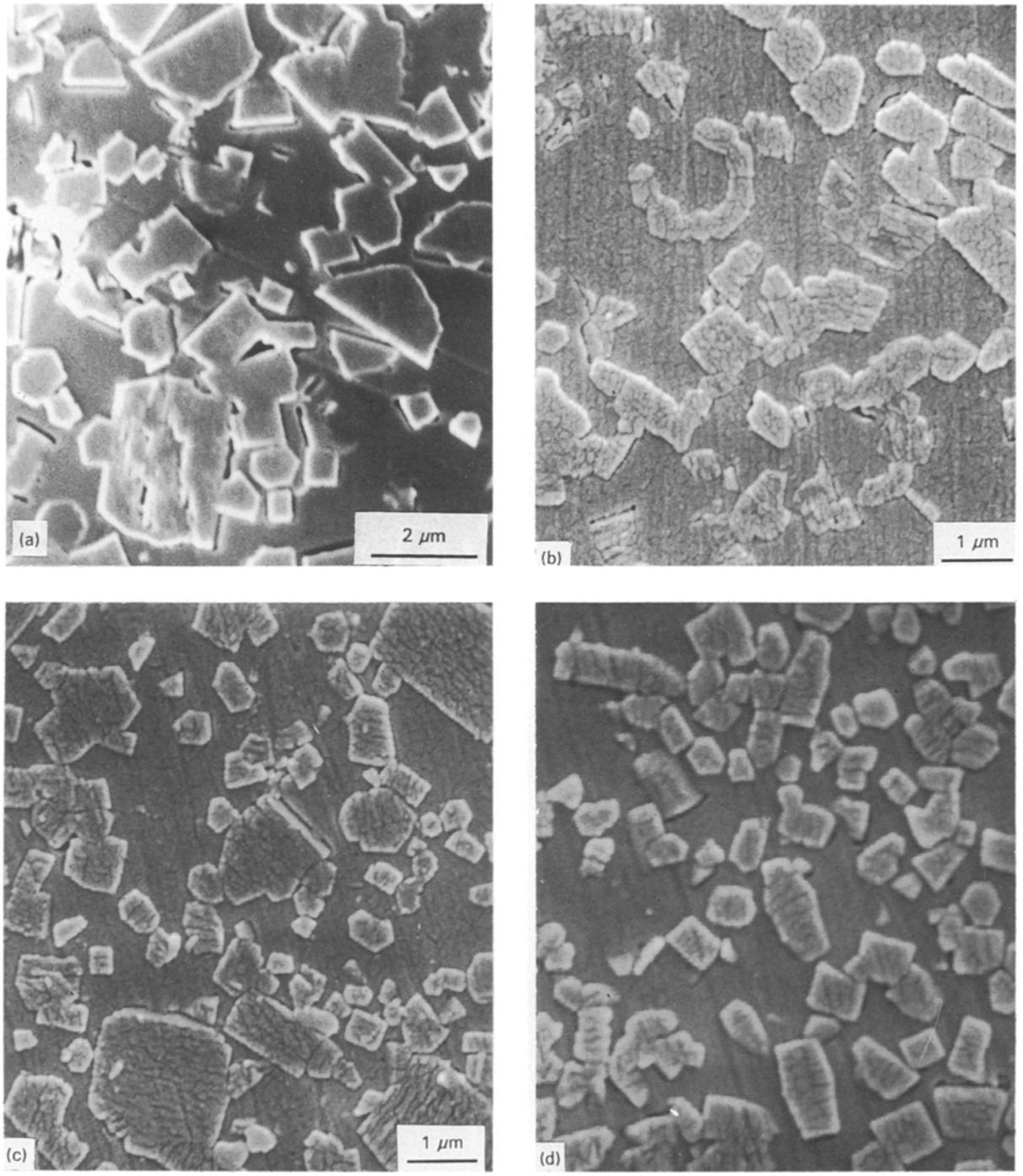

Figure 4 SEM surface morphology of as-cerammed DICOR-related glass. (a) DICOR, (b) SDICOR, (c) SDZR20, (d) SDAL100.

than other fine grains. As a result of rapid growth, the solute atoms are depleted, and the growth of grains near the abnormal grain is forbidden. Thus, a depleted zone is developed.

Chyung *et al.* [17] described the development of mica flakes as characterized by a large anisotropy of growth rate in the direction parallel and perpendicular to the basal plane. In a simple structure of fluorophlogpite crystal, the tightly bounded aluminosilicate sheets ($Mg_3(AlSi_3O_{10})F_2$) are weakly bound together by large 12-coordinated K^+ ions. When the composition is deficient in K^+ ions, the number of these weak bonds decreases. This favours the anomalously rapid growth of mica crystal in the direction parallel to the basal plane, and grains with large diameter and large aspect ratio are thus developed.

In addition to the pre-formed nuclei and grains contributing to the abnormal grains, inhomogeneity in the glass as well as a small concentration of impurity, especially for metal ion pollutants, will lead to an inhomogeneous microstructure of the glass-ceramics.

Fig. 6 shows the SEI image and X-ray maps near the abnormal grain region for SDICOR glass. Appreciable differences in concentrations of potassium and magnesium exist between matrix and the large-grain area. Magnesium-rich and potassium- depleted areas are observed in abnormal grains, as indicated in Fig. 6b and c. The difference in the weight ratio (K:Mg) between batch composition, and the stoichiometric ratio of mica crystal ($KMg_{2.5}Si_4O_{10}F_2$) is responsible for the variation in X-ray intensity. The ratio of (K:Mg) in mica crystal is around (1:1.55),

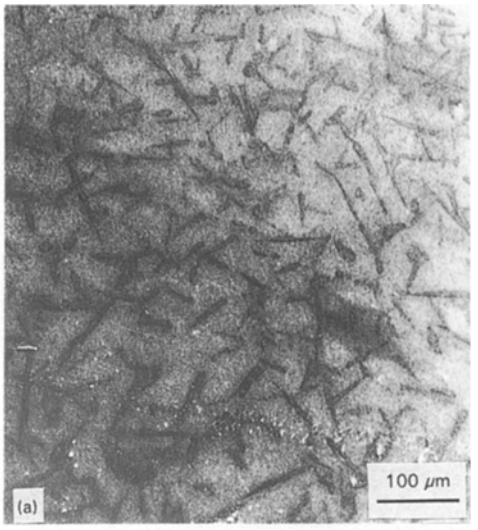

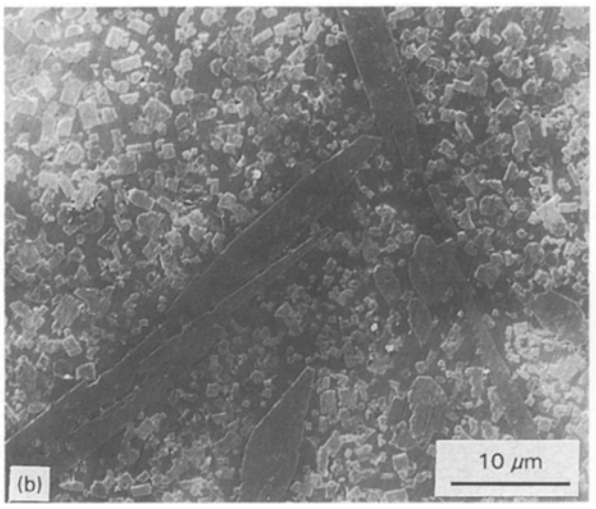

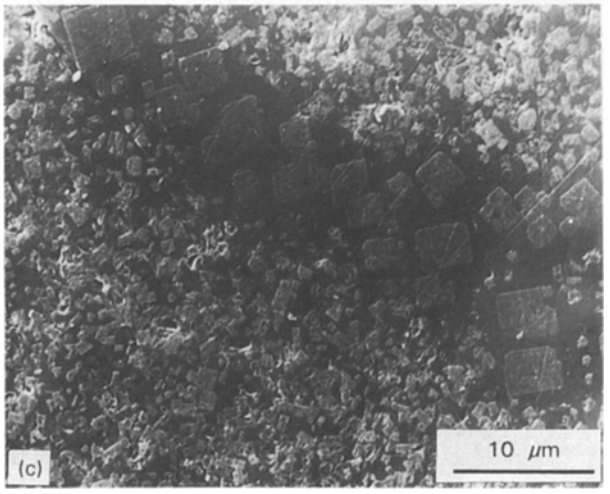

Figure 5 SEM surface morphology of SDICOR: (a) low magnification, (b, c) higher magnification.

while it is (1:0.9) for the batch composition. It is apparent that the batch composition contains less magnesium than that in the mica crystal.

3.4. Mechanical properties

Fracture strength and fracture toughness, K_{IC}, are very important parameters to decide whether the material is suitable for bio-medical application. In addition, surface hardness is an indication of wear resistance. Thus, mechanical strength, fracture toughness as well as hardness are the major concerns of mechanical properties in the development of glass-ceramics for dental application.

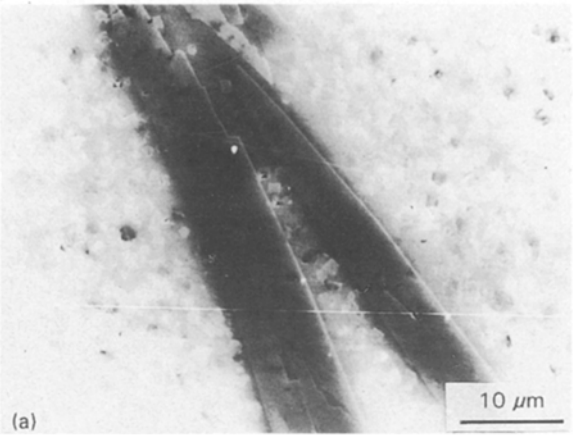

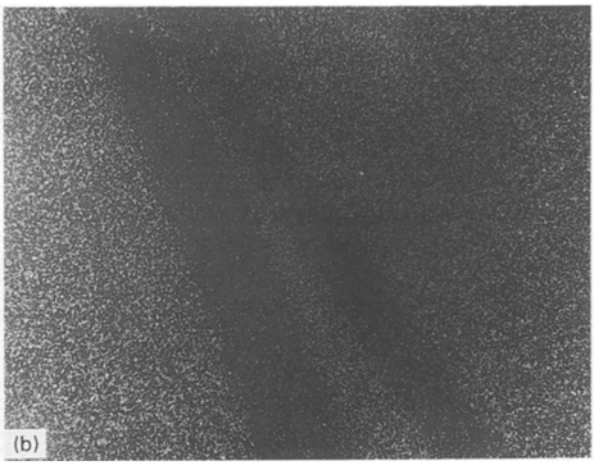

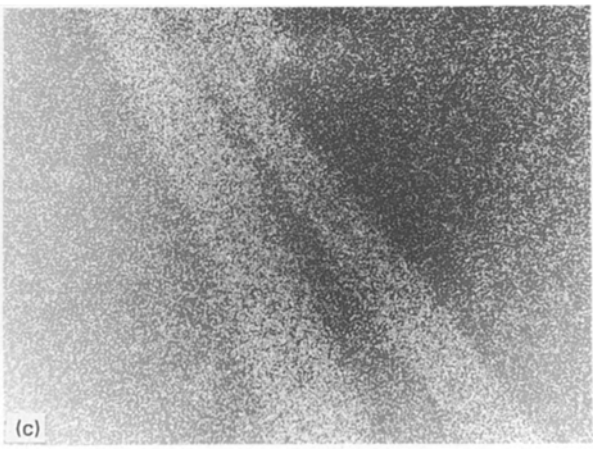

Figure 6 EPMA micrographs in the abnormal grain growth region for SDICOR: (a) SEI, (b) K X-ray map, (c) Mg X-ray map.

3.4.1. Effects of compositions on bending

The bending strength of material systems, employed in this study, are summarized in Table V. It appears that SDICOR, SDAL100, and SDAL200 exhibit higher fracture strengths than DICOR. It is interesting

TABLE V Bending strength of as-cerammed DICOR-related glass

Sample	σ_{3p}(MPa)	S.D. (MPa)
DICOR	109.2	8.8
SDICOR	115.7	5.6
SDZR05	73.7	9.7
SDZR10	105.4	14.3
SDZR20	67.4	47.8
SDAL100	126.1	17.4
SDAL200	127.5	13.5
SDAL300	106.1	16.4

to note that specimens SDAL100 and SDAL200 possess the highest bending strength, about 17% more than that of commercialized DICOR. This presents a favourable approach in the future development of bioglass ceramics. However, fracture strength decreases if extra ZrO_2 is added, as in the cases for SDZR05, SDZR10, and SDZR20.

According to Table IV, Al_2O_3 dopants lead to higher crystallization temperature than that of SDICOR. This is attributed to the incorporation of Al^{3+} ions into the glass and glass-ceramic networks. Aluminium forms tetrahedra in the multi-component glass. $[AlO_4]$ and $[SiO_4]$ tetrahedra are of similar sizes, so that in the silicate network, the former are capable of isomorphous partial substitution for the latter [18] with almost no stress induction. This results in a stronger and stable structure of glass-ceramic. Thus, addition of 100% or 200% extra Al_2O_3 into the original DICOR leads to a higher fracture strength. However, for 300% extra Al_2O_3 (SDAL300), the strength turns to a lower value than that of SDICOR. According to Table IV, T_c of SDAL300 is 834.5 °C, which implies that more aluminium take part in the network than in SDAL100 and SDAL200. This substitution of aluminium for silicon leads to a reduced stress because of lower single-bond strength of Al–O (79–101 kcal/g atom^{-1}) than Si–O (106 kcal/g atom^{-1}) [19]. In addition, the reduction in strength of SDAL300 may be derived from the formation of a lower strength fluorophlogopite ($KMg_3AlSi_3O_{10}F_2$) [17] because excess Al^{3+} replaces parts of Si^{4+} in a higher strength tetrasilicic. As a consequence, lower fracture strength results.

From Table V, the relatively low strength, 67.4 MPa, for SDZR20 may be attributed to the presence of abnormal grains in SDZR20, as indicated in Fig. 4c. The dark region in Fig. 5 represents the agglomeration of large grains. In addition to fine grains and glass matrix, abnormal grains play an important role in the microstructure. Because of strong anisotropy in thermal expansion ($\alpha_a = 69$, $\alpha_b = 55$, $\alpha_c = 198 \times 10^{-7}°C^{-1}$) of tetrasilicic mica crystal [17], the effects of thermal expansion mismatch become greater as the grain size increases. A weak interfacial bonding will be induced due to the thermal mismatch between glass and large grains. The weak interfaces provide a rather easy path for crack propagation and thus lower strength results. The fracture surface micrographs shown in Fig. 7 give evidence of the fracture path. In

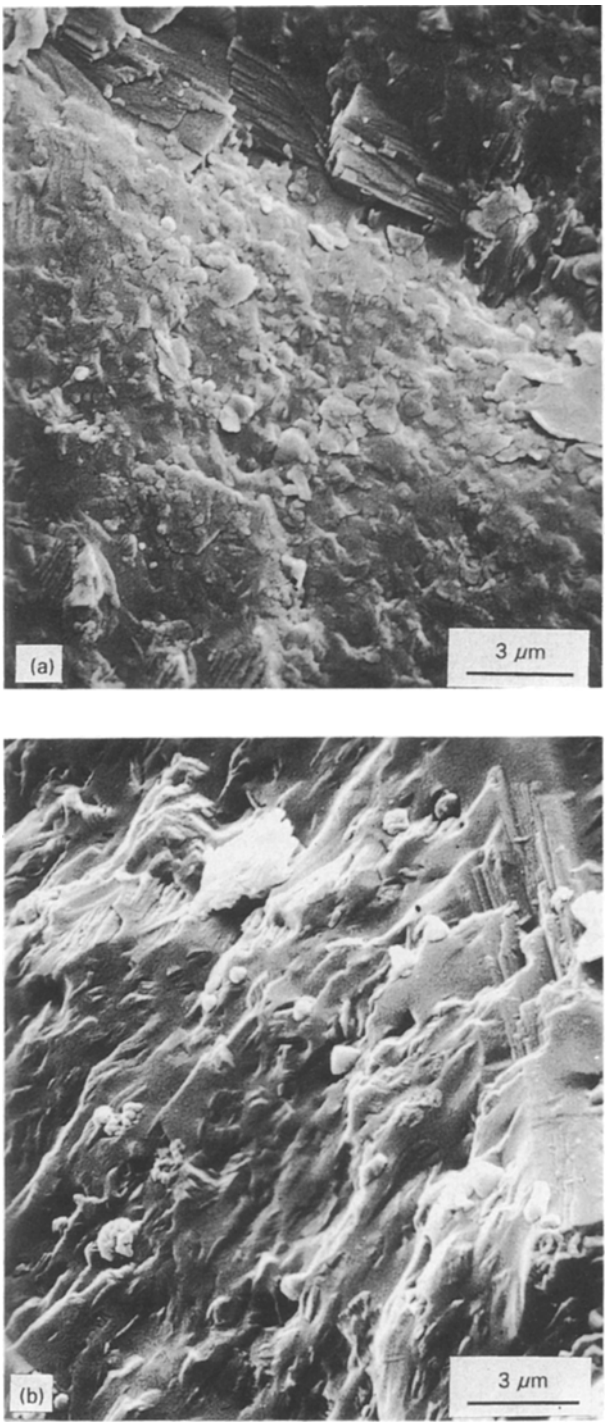

Figure 7 Scanning electron micrograph of ladder-like flakes on the fracture surface of SDZR20.

Fig. 7a, ladder-like flakes exist in the upper portion of the figure, which result from the fracture path across the interface between glass and abnormal grains. In addition to a weak interface, cleavage planes of mica crystals also lead to easy fracture propagation, especially for large grains. The upper right-hand side of Fig. 7b, exhibits fracture propagation along the cleavage plane of mica crystals. Combination of easy fracture propagation along cleavage planes of mica crystals and weak interfaces between glass matrix and mica grains, especially for abnormal grain, results in the lower strength in SDZR20 samples.

It was mentioned before that Al_2O_3 and ZrO_2 act as intermediate oxide which has been incorporated

into the glass network. The ionic radii of Zr^{4+} and Si^{4+} are 0.072, and 0.040 Mn [20], respectively. Tensile stress will be introduced in the matrix because much larger Zr^{4+} ions enter the silicon network, and strength is certainly decreased due to formation of tensile stress in the matrix. In addition to tensile stress induction, a lower single-bond strength of Zr–O (61–81 kcal/g.atom^{-1}) than that of Si–O (106 kcal/g atom^{-1}) may be another reason for the decrease in strength in the ZrO_2-doped DICOR system.

From another viewpoint, elastic modulus, E, may play an important role on the mechanical strength of the fabricated glass. Griffith postulated that the observed strength of glass, which was less than one-hundredth of its theoretical strength, was due to the presence of small cracks or flaws in glass [21]. Because the extremities of cracks have the ability to act as stress raisers, fracture occurs when the stress at the ends of the cracks exceeds the theoretical stress. On the basis of the Griffith equation [22]

$$\sigma = (2E\gamma/\pi c)^{1/2} \quad (2)$$

where σ is the mechanical strength, E the elastic modulus, γ the fracture surface energy, and c the length of the crack flaw. A higher E will lead to a better mechanical strength. It is reported that addition of Al_2O_3 increases the elastic modulus almost twice as much as SiO_2 [23]. This increase in elastic modulus has a favourable effect for Al_2O_3 on the mechanical strength according to Griffith's relationships. On the other hand, the modulus of elasticity of glass decreases with increasing ZrO_2 content [24]. The employment of elastic modulus may provide further evidence to explain the increase of fracture strength of the DICOR system due to additional Al_2O_3 dopants and the decrease of strength with increasing excess ZrO_2 dopants.

It should be pointed out that a number of pores exist on the fracture surface of the fabricated DICOR-related glass. In this study, the measured bending strength of commercial DICOR is around 110 MPa, which is, however, lower than the maximum value reported [25]. It is argued that this lower strength may be due to the presence of the porosity. These pores will not only reduce the effective area on which a load applies but also act as stress concentrators to decrease the strength, so a lower strength is obtained. These pores mainly come from a casting process in which bubbles are trapped in the ingot. In addition to the residual bubbles in the raw glass material, a large number of bubbles will form when the glass is melted. Most of the bubbles will vanish by floating to surface and then breaking, but some will still remain in the molten glass liquid and are trapped in the casting when casting is finished. In addition to reduce the pores present in the raw glass, holding for a longer time or increasing the casting temperature may be one of the alternatives to solve the problem.

3.4.2. Hardness

Hardness was evaluated by Knoop microhardness tests. Loads of 300 and 500 gf were employed for glass samples and as-cerammed samples, respectively. The holding time at the peak load was 15 s. The hardness of DICOR-related glasses are around 1760–1850 KH_v, and of as-cast samples are nearly 1720 KH_v. The Knoop hardness of selected systems, after ceramming are listed in Table VI.

The difference in hardness between raw glass and as-cerammed samples may be attributed to the large thermal stress induced during the glass-fabrication processes. Glass is produced through a rapid quenching of a molten liquid. A gradient in temperature will lead to a large thermal stress. The high Knoop hardness ($\sim$ 1800) of glass specimens may arise from the surface compression generated during fast cooling. The centre of the glass cools relatively slowly compared to the surface during rapid cooling and results in a difference in specific volume between the surface and interior. This causes the surface to be pulled into compression, and a residual compressive stress will form on the surface; consequently a very hard and brittle glass bulk is produced. However, a rather slow cooling rate which is used for heat treatment of glass-ceramics is to avoid excess cracks formed in the glass-ceramics due to thermal stress. Except for thermal mismatch due to the difference in thermal expansion coefficient between the crystalline phase and the glass phase, a stress relief glass-ceramic may be derived from an appropriate treatment. As a example, it takes DICOR 6 h to cool from 1065 °C to 200 °C, following furnace cooling to room temperature.

As indicated in Table VI, the measured hardness for DICOR is $\sim$ 400, which is approximately 10% higher than the proposed value, 362, by Dentisply International [12]. Other simulated system exhibit higher hardness than DICOR. This phenomenon may be related to a higher quantity of residual glass phase for the simulated glass. In general, a higher content of residual glass phase will lead to high hardness. Fig. 8 shows the Si NMR spectrum of DICOR and SDICOR. A broader shoulder appears around -97 p.p.m., which lies beside the peak position of -91.86 p. p. m. A shoulder with smaller count occurs on DICOR compared to SDICOR. The NMR spectrum implies that a lower degree of crystallization takes place on SDICOR than DICOR.

Glass-ceramic materials are composed of crystalline phase and residual glass phase. In addition to the crystalline phase, residual glass phase also plays an important part in the final properties, and the characteristics of a glass-ceramic are a compromise of prop-

TABLE VI Knoop hardness of as-cerammed Dicor-related glass

Sample	KH_v (kg mm^{-2})	S.D. (kg mm^{-2})
DICOR	401.1	9.9
SDICOR	445.5	15.8
SDZR05	445.2	13.8
SDZR10	448.8	15.4
SDZR20	469.3	5.7
SDAL100	452.9	9.8
SDAL200	457.4	11.0
SDAL300	442.9	10.4

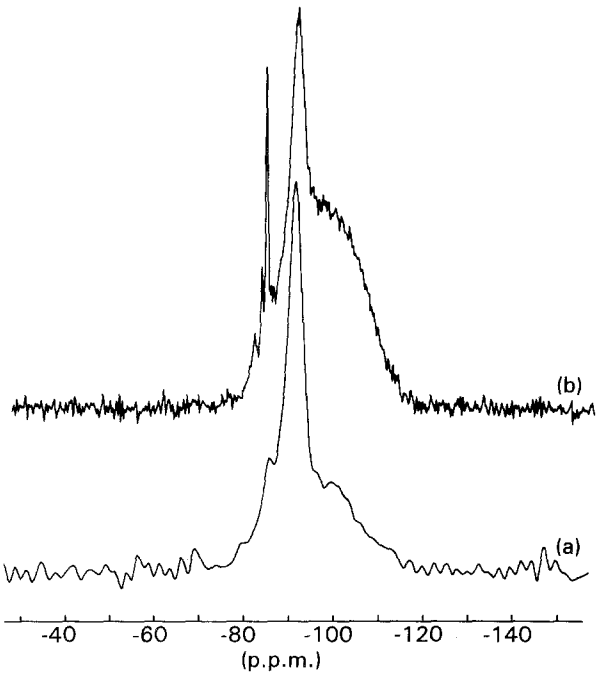

Figure 8 Si NMR spectrum curves for (a) DICOR, (b) SDICOR.

erties between the crystalline phase and the glass phase. Because the precipitated crystal possesses lower hardness than the glass matrix, lower degree of crystallization and consequently more residual glass phase lead to higher hardness in SDICOR, compared to original DICOR.

4. Conclusions

1. A series of simulated formulations to commercial DICOR dental material have been proposed. Appropriate amounts of K_2O, MgO, MgF_2, SiO_2, ZrO_2, and Al_2O_3 were melted at elevated temperature and then quenched to form glass, which was further cerammed to derive the glass-ceramics.

2. Tetrasilicic fluorine mica crystal ($KMg_{2.5}Si_4O_{10}F_2$) phase formed in all the DICOR-modified glass-ceramics. DICOR-related glass-ceramics exhibit a property of machinability due to the uniformly dispersed and interlock mica crystals.

3. Appropriate additions of Al_2O_3 led to an increase in bending strength because aluminium stabilizes and strengthens the DICOR-related glass-ceramics by being incorporated into the silicon network.

4. Extra ZrO_2 addition to DICOR formulation resulted in a decrease in strength. This is attributed to larger zirconium ionic radius and lower bond strength of Zr–O in the silicon network. The decrease in strength may also be related to the decrease of modulus of elasticity in glass with increasing contents of ZrO_2.

Acknowledgements

This research was sponsored by the National Tsing Hua University, Hsinchu, and Veterans General Hospital, Taipei under the contracts VGHTH-78-020-1 and VGHTH-80-032-1 (Medical Research Advancement Foundation in memory of Dr Chi-Shuen Tsou).

References

1. D. G. GROSSMAN and H. WALTERS, *J. Dent. Res.* **63** (1984) 234.
2. S. F. HULBERT, L. L. HENCH, K. FORBES, and L. S. BRWMAN, in "Ceramic in Surgery", edited by P. Vincenzini (Elsevier Science, New York, 1983) p. 3.
3. W. J. McLEAN, *Brit. Dent. J.*, **164** (1988) 1887.
4. W. T. MacCULLOCH, *ibid.* **124** (1968) 361.
5. L. L. HENCH, *et al.* J. Dent. Res. **50** (1971) 133.
6. D. J. ADAIR, US Pat. 4431420, 14 February 1984, US, Patent Office, Washington, D. C.
7. D. G. GROSSMAN, US Pat. 3839055, 1 October, 1974, US, Patent Office, Washington, D. C.
8. *Idem, J. Can. Ceram. Soc.* **55** (1972) 446.
9. S. F. ROSENSTIEL, and S. S. PORTER, *J. Pros. Dent.*, **62** (1989) 529.
10. D. J. GREEN, R. H. J. HANNIND, and M. V. SWAIN,in "Transformation Toughening of Ceramics" (CRC Press, Florida, 1989) Ch. 3.
11. J. G. DUH, H. T. DAI and B. S. CHIOU, *J. Am. Ceram. Soc.* **71** (1988) 813.
12. "Installation Operation and Service Manual of DICOR", Dentsply International and Corning Glass Works. York, PA, USA (1987).
13. F. SEIFERT and W. SCHREYER, *Am. Mineral.* **50** (1965) 1114.
14. J. M. TZENG, MS thesis, National Tsing Hua University, Hsinchu, Taiwan (1990)
15. F. de MESTRAL and R. A. L. DREW, *J. Eur. Ceram. Soc.* **5** (1989) 47.
16. J. S. OLCOTT and S. D. STOOKEY, US Pat. 2998675, 5 September, 1961, US Patent Office Washington, D. C.
17. C. K. CHYUNG, F. J. BEALL and D. G. GROSSMAN, in "Electron Microscopy and Structure of Materials", edited by G. Thomas (University California Press, Berkeley, 1971) pp. 1167–94.
18. M. B. VOLF, in "Chemical Approach to Glass" (Elsevier, Amsterdam, 1984) Ch. 14.
19. W. D. KINGERY, H. K. BOWEN, and D. R. UHLMANN, in "Introduction to Ceramics", 2nd Edn (Wiley, New York, 1976) Ch. 3.
20. R. D. SHANNON and C. T. PREWITT, *Acta Crystallog.* **B25** (1969) 925.
21. A. A. GRIFFITH, *Phil. Trans. R. Soc.* **a221** (1924) 163.
22. R. E. REED-HILL and R. ABBASCHIAN, in "Physical Metallurgy Principles", 3rd Edn (PWS-KENT, Boston, MA, 1992) Ch. 22.
23. M. B. VOLT, in "Chemical Approach to Glass" (Elsevier, Amsterdam, 1984) Ch. 16.
24. M. NOGAMI and K. NAGASKA, *J. Non-Cryst. Solid*, **100** (1988) 298.
25. J. R. KELLY, S. D. CAMPBELL and H. K. BOWEN, *J. Pros. Dent.* **62** (1989) 536.

Received 28 July 1992
and accepted 19 March 1993